

# **SCALE-UP OF REACTIVE DISTILLATION COLUMNS WITH CATALYTIC PACKINGS**

**Achim Hoffmann, Christoph Noeres, Andrzej Górak**

Department of Chemical Engineering, Dortmund University, 44221 Dortmund,  
Germany

## **ABSTRACT**

The scale-up of reactive distillation columns with catalytic packings requires the knowledge of reaction kinetics, phase equilibrium and packing characteristics. Therefore, pressure drop, liquid holdup and separation efficiency have been determined for the catalytic packing MULTIPAK<sup>®</sup>. A new hydrodynamic model that describes the counter-current gas-liquid flow for the whole loading range and considers the influence of the column diameter has been implemented into a rate-based column model. Simulation results for the methyl acetate synthesis are compared with pilot plant experiments that cover a wide range of different process conditions. The experiments are in good agreement with the simulation results and confirm the applicability of the modelling approach for reactive distillation processes with catalytic packings.

## **INTRODUCTION**

The combination of heterogeneously catalysed reaction and separation in one single process unit, known as catalytic distillation, is one of the most common applications of the multifunctional reactor concept [1]. In comparison to the conventional approach, where reaction and separation are carried out sequentially, catalytic distillation can considerably improve the process performance [2,3]. One of the advantages is the elimination of equipment for product recovery and recycling of unconverted reactants, which leads to savings in investment and operating costs. Catalytic distillation may also improve selectivity and mass transfer and avoid catalyst fouling [4]. Even if the invention of catalytic distillation dates back to 1966 [5], the number of processes in which catalytic distillation has been implemented on a commercial scale is still quite limited but the potential of this technique goes far beyond today's applications [6].

Different process configurations can be chosen to carry out catalytic distillation [7]. The installation of a solid catalyst inside a distillation column attains the largest

extend of process intensification, but on the other hand substantially complicates the design of catalytic distillation processes. Especially the choice of suitable catalytic column internals is one of the major problems. Those devices have to reconcile satisfactory separation efficiency and catalytic activity without limiting possible column loads. Catalyst bales have been used successfully in commercial scale MTBE production, but high-capacity devices can lower capital costs for catalytic distillation columns [8]. However, designing a catalytic distillation column requires knowledge of device characteristics as well as of reaction kinetics, chemical and vapour-liquid equilibrium [9]. Thus, a suitable model is indispensable to reflect the complex behaviour of catalytic distillation columns [10].

In recent years, great effort has been made to investigate the relevant phenomena occurring in catalytic distillation processes. The analysis of reactive distillation processes from a thermodynamic point of view, as done by Doherty and Buzad [11], Nisoli et al. or Frey and Stichlmair [12], allows to identify the presence of reactive azeotropes and to check the feasibility of the process. Okansinski and Doherty [13] outlined the important role of uncertainties in model parameter at this early stage of process design. Models of different complexity have been presented to describe the behaviour of catalytic distillation processes [14]. Bessling et al. [15] analysed the process of methyl-acetate synthesis via catalytic distillation using a simple model assuming chemical and vapour-liquid equilibrium on all stages. A steady-state rate-based model for the production of diacetone alcohol with catalytic distillation was developed by Podrebarac et al. [16]. Higler et al. [17] and Kenig et al. [18] presented a non-equilibrium model for reactive distillation columns using the Maxwell-Stefan approach to describe the mass-transfer between vapour and liquid phase. Sundmacher and Hoffmann [19] proposed a detailed non-equilibrium model including the mass transfer resistance between the liquid phase and the porous catalyst for the MTBE process. Bart and Landschützer [20] analysed the influence of axial dispersion and varying model parameter on the performance of catalytic distillation columns. Schneider et al. [21] developed a dynamic model for the production of methyl-acetate using reactive batch distillation. A comparison between equilibrium and non-equilibrium models for reactive distillation columns by Lee and Dudukovic [22] showed that the reaction rate is the main factor that affects the column behaviour, a fact that was also pointed out by Podrebarac et al. [23]. Subwalla and Fair [24] used an equilibrium stage model to derive design guidelines for catalytic distillation systems considering several key design parameters such as pressure, reactive zone location, reactant feed ratio, feed location, amount of catalyst, column diameter and number of equilibrium stages in reactive and non-reactive zones, but they recommend the use of a rate-based model to determine the height of the column.

Extensive experimental work has been performed to investigate the behaviour of reactive column internals. The hydrodynamics of catalyst bales used for MTBE production have been determined by Zheng and Xu [25], Xu et al. [26] and Subwalla et al. [27] while Huang et al. [28] investigated the mass transfer behaviour of a laboratory-scale packing for the aldol condensation. Several investigations concerning the hydrodynamic behaviour of the catalytic packing Katapak<sup>®</sup>-S have been presented by Moritz et al. [29], Moritz and Hasse [30] as well as Ellenberger and Krishna [31]. Device characteristics of the structured catalytic packing MULTIPAK<sup>®</sup> [32] have been published by Kreul [33], Górak and Hoffmann [9] and Noeres et al. [34]. Since reaction kinetics have been recognised as a model-

parameter of great influence, they have been determined experimentally for different catalytic distillation processes. The synthesis of methyl acetate mentioned in this study has been investigated by Xu and Chuang [35,36] and Pöpken et al. [37,38].

The objective of this contribution is to provide information for the design of reactive distillation columns with the catalytic packing MULTIPAK<sup>®</sup>. Therefore a hydrodynamic model was derived on the basis of experimental data for pressure drop and liquid-holdup that describes the countercurrent gas-liquid flow for the whole loading range of the packing and considers the influence of the column diameter. A comparison of model-prediction and experimental data for different types of MULTIPAK<sup>®</sup> is presented in this paper. Data for the separation efficiency of MULTIPAK<sup>®</sup>, which has been published previously [9], completes the set of essential model parameter for the design of catalytic distillation columns. This information is incorporated into a non-equilibrium model for reactive distillation columns using the Maxwell-Stefan equations to describe mass-transfer between vapour and liquid phase. Simulation results are compared with new experimental data for the synthesis of methyl acetate that cover a wide range of process conditions.

### **STRUCTURED CATALYTIC PACKING MULTIPAK<sup>®</sup>**

The catalytic packing MULTIPAK<sup>®</sup> has been developed in consideration of the qualities of modern structured wire gauze packings and their improvements on conventional distillation. Figure 1 shows one packing element of MULTIPAK<sup>®</sup> with a packing diameter of 100 mm. It consists of corrugated wire gauze sheets and catalyst bags of the same material assembled in alternate sequence. This construction enables high column loads by providing open channels for the gas flow while most of the liquid is flowing downwards through the catalyst bags. Sufficient mass transfer between gas and liquid phase and radial mixing is guaranteed by the segmentation of the catalyst bags and numerous contact spots with the wire gauze sheets. The catalyst bags can be filled with different types of particle shape catalyst, in case of the methyl acetate synthesis an acidic ion exchange resin (Lewatit K2621, Bayer AG) was used.



*Figure 1: Packing element of MULTIPAK<sup>®</sup>.*

## Characteristic Geometric Data

Two different types of MULTIPAK<sup>®</sup> can be distinguished. The layers of corrugated wire gauze sheets of MULTIPAK<sup>®</sup>-I have an inclination angle of 60 degrees and a specific surface area of 500 m<sup>2</sup>/m<sup>3</sup> while MULTIPAK<sup>®</sup>-II comprises of sheets with an inclination of 45 degrees and a specific surface area of 750 m<sup>2</sup>/m<sup>3</sup>. Catalyst bags used for MULTIPAK<sup>®</sup>-II are thicker than for MULTIPAK<sup>®</sup>-I and allow a higher catalyst volume fraction in combination with a reduced specific surface area. Therefore, specific requirements of the process can be taken into account by choosing the packing type. To ensure a similar hydrodynamic behaviour of laboratory and technical scale packings, both consist of the same elements. However, weld joints at the edges of the catalyst bags and the gap between the packing and the column wall result in less catalyst volume fraction, less specific surface area and a higher void fraction for laboratory scale packings. This has to be considered for the scale-up of reactive distillation processes with MULTIPAK<sup>®</sup>. The characteristic geometrical data for the two different types of MULTIPAK<sup>®</sup> as a function of the column diameter are shown in Figure 2.

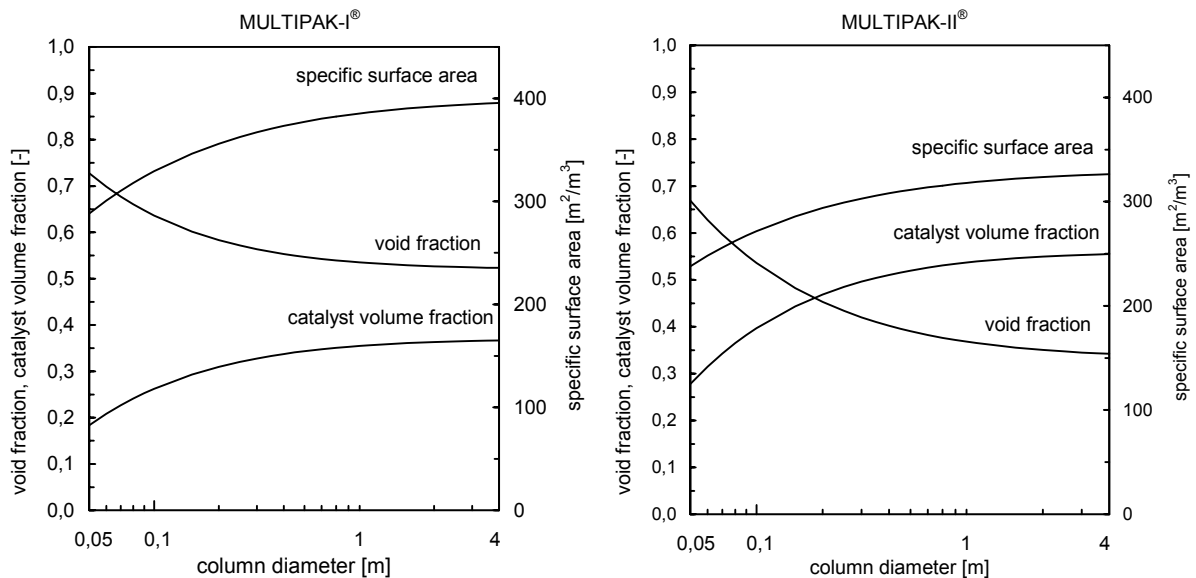


Figure 2: Characteristic geometric data of MULTIPAK<sup>®</sup>.

## Flow Regimes

Moritz et al. [29] identified different flow regimes for the catalytic structured packing Katapak<sup>®</sup>-S in dependency on the liquid load. They defined a maximum liquid velocity  $u_{L,max}$  for the catalyst bags which depends on the physical properties of the liquid and the properties of the catalyst bed in terms of the particle size  $d_p$  and the void fraction of the bed  $\varepsilon_{CB}$ . If the liquid load is lower than the maximum value, the catalyst particles are generally completely wetted because of their small size, but the space between them is not totally filled with liquid. Capillary effects draw the liquid into the catalyst bags, where it flows downwards and trickles out at the bottom of the bags. At liquid loads above the maximum value, the catalyst bags are completely filled with liquid and the excess liquid will flow outside the bags as bypass.

Even if the structure of MULTIPAK<sup>®</sup> differs significantly from Katapak<sup>®</sup>-S, these flow regimes can also be observed, as shown in Figure 3. For liquid loads below  $u_{L,max}$  liquid is perceptible only between the segments of the catalyst bag, while the bypass flow is clearly visible for higher loads. Due to the segmentation of the catalyst bags, MULTIPAK<sup>®</sup> guarantees frequent remixing of the liquid and contact between the phases even at very low liquid loads.

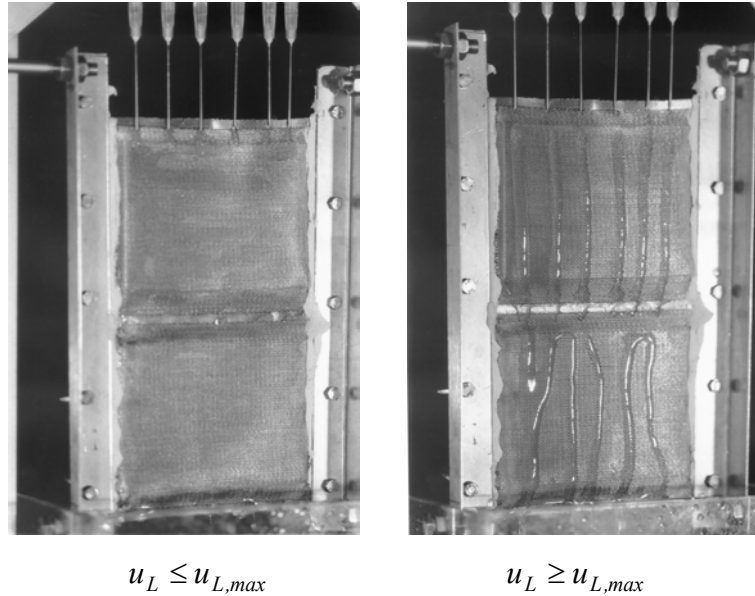


Figure 3: Flow regimes of MULTIPAK<sup>®</sup>.

The maximum liquid load can be calculated according to the method of Moritz et al. [29], which was adapted for MULTIPAK<sup>®</sup> to give

$$u_{L,max} = \frac{\varepsilon_{CB}^3}{1 - \varepsilon_{CB}} \cdot \frac{g \cdot d_P}{\xi_{CB}} \quad (1)$$

with

$$\xi_{CB} = \frac{160}{Re_{LP}} + \frac{3.1}{Re_{LP}^{0.1}} \quad (2)$$

and

$$Re_{LP} = \frac{u_{L,max} \cdot d_P \cdot \rho_L}{(1 - \varepsilon_{CB}) \cdot \eta_L} \quad (3)$$

The results of these calculation were compared with experimental results for different liquids as shown in Figure 4. It can be seen that the data agrees with a maximum deviation of  $\pm 20\%$ , but one has to be aware that the maximum liquid velocity strongly depends on the particle size and the void fraction of the catalyst bed. Since these values are not known with high accuracy, especially for catalysts like ion exchange resins whose swelling behaviour strongly depends on the liquid phase composition, there are serious uncertainties in determining the maximum liquid velocity under process conditions. Moritz and Hasse [39] recently stated that catalytic packings can be operated well above this liquid load and therefore emphasised the demand for a hydrodynamic model that describes the flow behaviour for the whole loading range of the packing.

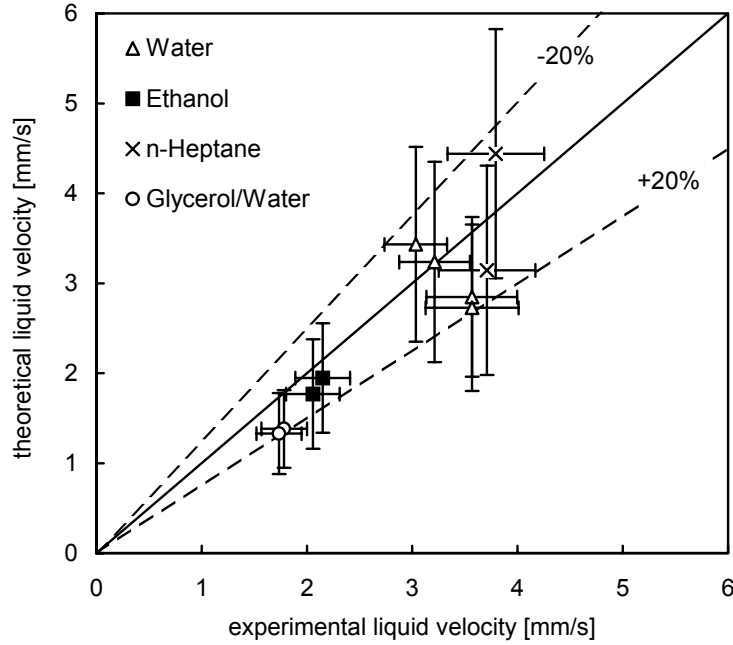


Figure 4: Maximum liquid velocity inside the catalyst bags.

### HYDRODYNAMIC MODEL FOR MULTIPAK®

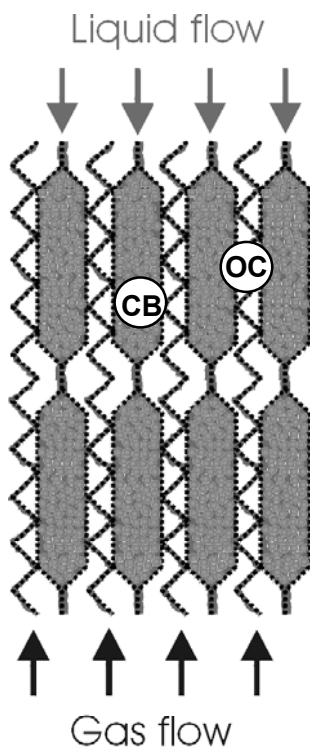


Figure 5: Hydrodynamic modelling.

The hydrodynamic model for MULTIPAK® reflects the geometric structure of the packing which consists of catalyst bags (CB) and open channels (OC) as shown in Figure 5. The model is based on the following assumptions:

- Gas flows only through the open channels OC
- Liquid flows through the open channels OC and the catalyst bags CB
- The liquid flow through the catalyst bags is limited to a maximum velocity given by equations 1-3
- Liquid holdup in the open channels increases the resistance to the gas flow

According to these assumption, the liquid flow is divided into one part for the catalyst bags  $u_{L,CB}$  and a second for the open channels  $u_{L,OC}$ . They are connected by

$$u_L = u_{L,CB} \cdot \psi + u_{L,OC} \cdot \varepsilon \quad (4)$$

The liquid velocity inside the catalyst bags can be calculated as

$$u_{L,CB} = \frac{u_L}{\varepsilon + \psi} \quad \text{if} \quad u_L \leq u_{LP} \quad (5)$$

$$\text{and} \quad u_{L,CB} = u_{L,max} \quad \text{if} \quad u_L \geq u_{LP} \quad (6)$$

The change in flow regime takes place at the “load point” which is determined by

$$u_{LP} = u_{L,max} \cdot (\varepsilon + \psi) \quad (7)$$

### Liquid Holdup

The liquid holdup for MULTIPAK® can be divided in three different parts, which add up to the total value.

a) Catalyst bags  $0 \leq h_{L,CB} \leq \psi \cdot \varepsilon_{CB}$  (8)

b) Open channels  $0 \leq h_{L,OC} \leq \varepsilon$  (9)

c) Wire gauze sheets  $0 \leq h_{L,CB} \leq (1 - \psi - \varepsilon) \cdot \varepsilon_{WG}$  (10)

Since only the total liquid holdup can be determined experimentally, experimental data for liquid loads above the load point were used to derive the liquid holdup inside the open channels, assuming that the catalyst bags are completely filled and the wire gauze sheets are totally wetted. Gas loads were chosen small enough to ensure that there is no mutual influence of gas and liquid flow. These data can be correlated in the well known form

$$h_{L,OC,0} = A \cdot Fr_{L,OC}^B \quad (11)$$

proposed by Mackowiak [40]. The Froude-Number for the open channel is given by

$$Fr_{L,OC} = \frac{u_{L,OC}^2 \cdot a}{g \cdot \sin \theta} \quad (12)$$

Assuming complete wetting of the wire gauze sheets, the liquid holdup inside the catalyst can be calculated from experimental data and represented by

$$h_{L,CB} = \psi \cdot \varepsilon_{CB} \cdot \left[ 1 - 0.5 \cdot \left( 1 - \frac{u_L}{u_{LP}} \right)^2 \right] \quad \text{if } u_L \leq u_{LP} \quad (13)$$

and  $h_{L,CB} = \psi \cdot \varepsilon_{CB}$  if  $u_L \geq u_{LP}$  (14)

Stichlmair et al. [41] propose an equation to describe the mutual influence of gas- and liquid flow up to the flooding point, that is also applicable to MULTIPAK®. The total liquid holdup of MULTIPAK® therefore can be calculated from

$$h_L = \psi \cdot \varepsilon_{CB} \cdot \left[ 1 - 0.5 \cdot \left( \frac{u_L}{u_{LP}} \right)^2 \right] + (1 - \varepsilon - \psi) \cdot \varepsilon_{WG} + A \cdot \left[ 1 + C \cdot \left( \frac{\Delta p}{\Delta z \cdot \rho_L \cdot g} \right)^2 \right] \cdot Fr_{L,OC}^B \quad (15)$$

below the load point and

$$h_L = \psi \cdot \varepsilon_{CB} + (1 - \varepsilon - \psi) \cdot \varepsilon_{WG} + A \cdot \left[ 1 + C \cdot \left( \frac{\Delta p}{\Delta z \cdot \rho_L \cdot g} \right)^2 \right] \cdot Fr_{L,OC}^B \quad (16)$$

above.

Figure 6 shows a comparison between experimental holdup data and theoretical results for MULTIPAK®-II with a packing diameter of 100 mm.

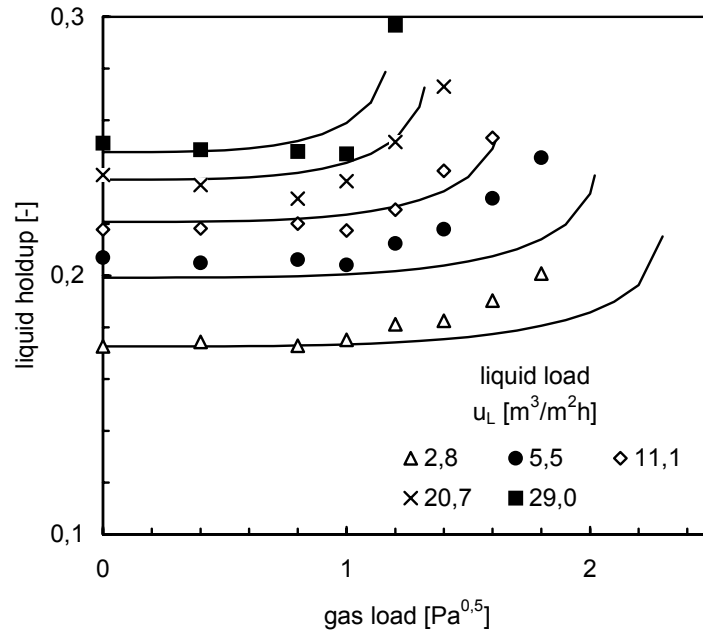


Figure 6: Liquid holdup of MULTIPAK®-II, DN 100.

### Pressure Drop

The calculation of liquid holdup for the whole loading range requires the knowledge of the pressure drop as a function of gas and liquid load. This has been determined experimentally. The pressure drop of the dry packing can be calculated according to the channel model proposed by Billet [42].

$$\frac{\Delta p_0}{\Delta z} = \xi(Re_G) \cdot \frac{a}{\varepsilon^3} \cdot \left( \frac{u_G}{\sin \theta} \right)^2 \cdot \frac{\rho_G}{f_s} \quad (17)$$

with 
$$\xi(Re_G) = D + \frac{E}{Re_G} \quad (18)$$

$$Re_G = \frac{u_G \cdot d_{eq} \cdot \rho_G}{\varepsilon \cdot \sin \theta \cdot \eta_G \cdot f_s} \quad (19)$$

$$d_{eq} = \frac{4 \cdot \varepsilon}{a} \quad (20)$$

and 
$$\frac{1}{f_s} = 1 + \frac{4}{a \cdot d_C} \quad (21)$$

The pressure drop of the irrigated packing is given by [43]

$$\frac{\Delta p}{\Delta p_0} = \left( \frac{1}{1 - F \cdot h_{L,OC}} \right)^5 \quad (22)$$

Figure 7 shows a comparison of experimental pressure drop data and theoretical results for MULTIPAK<sup>®</sup>-II with a packing diameter of 100 mm.

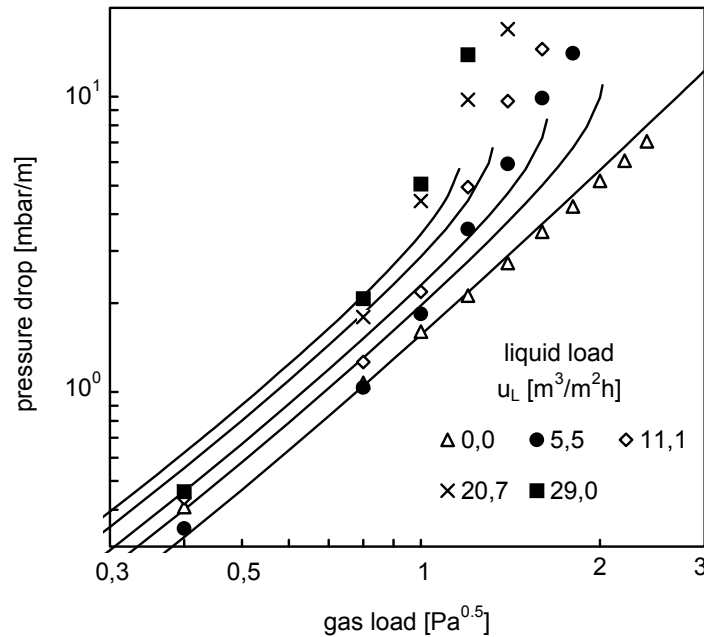


Figure 7: Pressure drop of MULTIPAK<sup>®</sup>-II, DN 100.

It can be seen that the proposed hydrodynamic model for MULTIPAK<sup>®</sup> reflects the flow behaviour with good accuracy. Information about the geometrical structure of the packing is included in the model and therefore the influence of column diameter can be considered for scale-up purposes. The loading limits of the packing are predicted without any additional correlation for the flooding point.

### Separation Efficiency

Besides pressure drop, liquid holdup and loading range, the separation efficiency of the packing plays an important role in the design of catalytic distillation columns. Therefore, distillation experiments have been carried out with the test system chlorobenzene / ethylbenzene, which has been recommended by Onken and Arlt [44] as a mixture for testing column internals at atmospheric pressure or vacuum. A distillation column with a diameter of 100 mm was equipped with 2 m of MULTIPAK<sup>®</sup>-I and operated with total reflux. The column load was changed by varying the heat duty and the operating pressure from 10 to 60 kPa to cover the whole loading range of the packing. When steady-state conditions were reached, liquid samples were taken directly above and below the catalytic packing and analysed via gas chromatography. The separation efficiency characterised by the number of theoretical stages can be calculated from the Fenske-equation [45].

$$n_{th} = \frac{I}{\ln \alpha} \cdot \ln \left( \frac{x_D}{x_B} \cdot \frac{I - x_B}{I - x_D} \right) \quad (23)$$

The application of Eq. (23) is limited to ideal binary systems, for the used test system this requirement is only fulfilled for operating pressures above 40 kPa. However, for lower operating pressures the deviation from a mean relative volatility  $\bar{\alpha}$  is below

0.2% [44]. Eq. (23) is therefore used for all operating pressures with a mean relative volatility calculated by

$$\bar{\alpha} = \exp \int_{x_B}^{x_D} \ln \alpha(x) dx \quad (24)$$

The number of theoretical stages per meter of the catalytic packing *NTSM*, is given by

$$NTSM = \frac{n_{th}}{H} \quad (25)$$

Figure 8 shows the *NTSM*-value of packing A as a function of the gas load, given by the F-Factor. For the whole range of column loads, the separation efficiency is at least 4 theoretical stages per meter. It remains constant for a wide loading range, but increases up to *NTSM* = 6 for lower column loads. This phenomenon was already reported by Pelkonen et al. [46] for the conventional structure packing Montzpak A3-500 whose corrugated wire gauze sheets are identical with MULTIPAK®-I. Moritz and Hasse [30] determined a value of *NTSM* = 3 for the laboratory-scale KATAPAK®-S.

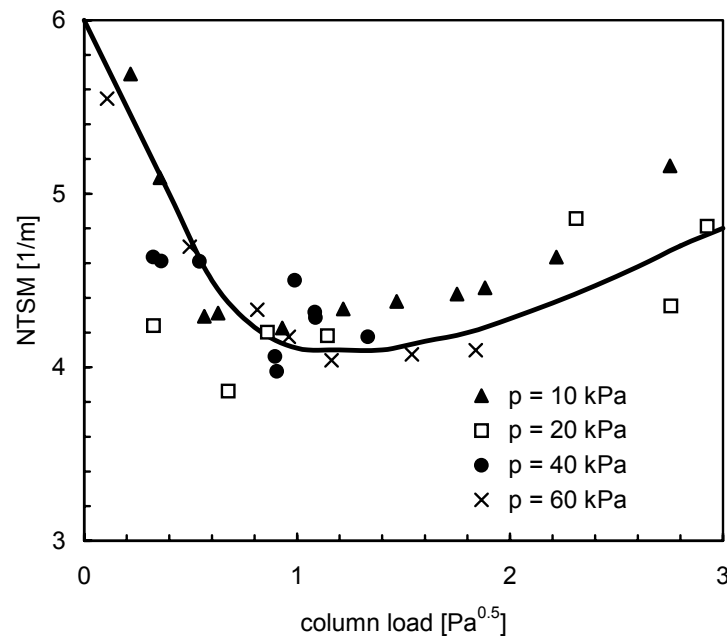


Figure 8: Separation efficiency of MULTIPAK®.

To enable the use of a non-equilibrium stage model for the design of reactive distillation columns equipped with MULTIPAK®, mass transfer coefficients and their dependence on column loads have to be available. They can be determined from the total reflux distillation experiments described above. Following the concept of transfer units [47], an overall mass transfer coefficient can be calculated from

$$k_{OG} = \frac{4 \cdot \dot{L}}{\pi \cdot c_{t,G} \cdot d_C^2 \cdot a \cdot H} \left[ \frac{1}{\alpha - 1} \ln \left( \frac{x_D}{x_B} \cdot \frac{1 - x_B}{1 - x_D} \right) + \ln \left( \frac{1 - x_B}{1 - x_D} \right) \right] \quad (26)$$

According to the generally adopted two-film theory, the relationship between the overall height of the gas phase transfer unit  $HTU_{OG}$  and individual film transfer unit  $HTU_G$  and  $HTU_L$  is given by

$$HTU_{OG} = HTU_G + m \cdot HTU_L \quad (27)$$

Even if the mass transfer resistance in the liquid phase is almost negligible in most distillation applications [48], the penetration approach is widely used to calculate the liquid phase mass transfer coefficient. It can be calculated from [49]

$$\beta_L = 2 \sqrt{\frac{0.9 \cdot D_L \cdot u_{L,eff}}{\pi \cdot S}} \quad (28)$$

with the effective liquid velocity defined as

$$u_{L,eff} = \frac{u_L}{\varepsilon \cdot h_L \cdot \sin \theta} \quad (29)$$

Assuming that this approach is also suitable for the catalytic packing due to the similar geometry of the gas-liquid flow channels, the vapour phase mass transfer coefficient can be calculated from

$$\beta_G = \frac{k_{OG}}{1 - m \cdot \frac{k_{OG} \cdot u_L}{\beta_L \cdot u_G}} \quad (30)$$

The experimental values of vapour phase mass transfer coefficients have been correlated in the well known form of dimensionless groups. The following correlation

$$Sh_G = 0.0064 \cdot Re_{G,eff}^{0.96} \cdot Sc_G^{0.33} \quad (31)$$

reproduces all experimental data within an accuracy of 15% as shown in Figure 9.

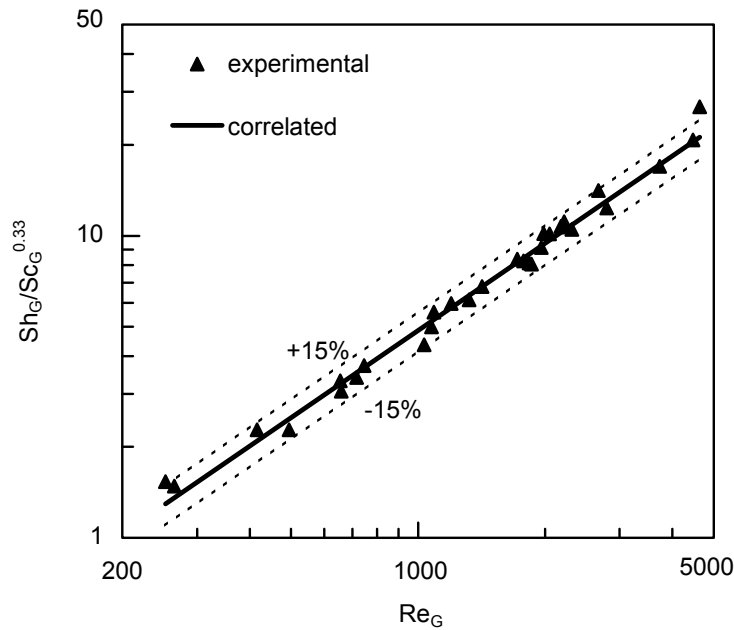


Figure 9: Vapor phase mass transfer coefficients.

The dimensionless groups have been defined according to Rocha et al. [49].

$$Re_{G,eff} = \frac{(u_{G,eff} + u_{L,eff}) \cdot S \cdot \rho_G}{\eta_G} \quad (32)$$

and 
$$Sc_G = \frac{\eta_G}{D_G \cdot \rho_G} \quad (33)$$

with 
$$u_{G,eff} = \frac{u_G}{\varepsilon \cdot (1 - h_L) \cdot \sin \theta} \quad (34)$$

## PROCESS MODELLING

A rigorous dynamic model for catalytic distillation processes has been presented by Schneider et al. [21] combining the dynamic balance equations required for batch operation and the rate-based approach for the appropriate description of multicomponent mass transfer. This model has been modified by implementing the hydrodynamic model for the catalytic packing MULTIPAK<sup>®</sup>.

The reactive distillation column was subdivided into a number of segments. The model for each segment  $j$  is based on the two-film theory [50] and consists of an ideally mixed vapour and liquid bulk phase and two film regions adjacent to the interface as shown in Figure 10. The catalysed reaction has been considered as quasi-homogeneous with no mass transfer resistance between liquid phase and catalyst. This assumption has already been described as justified for the synthesis of methyl acetate by several authors [51,52]. However, sorption effects inside the ion-exchange catalyst should not be neglected [33].

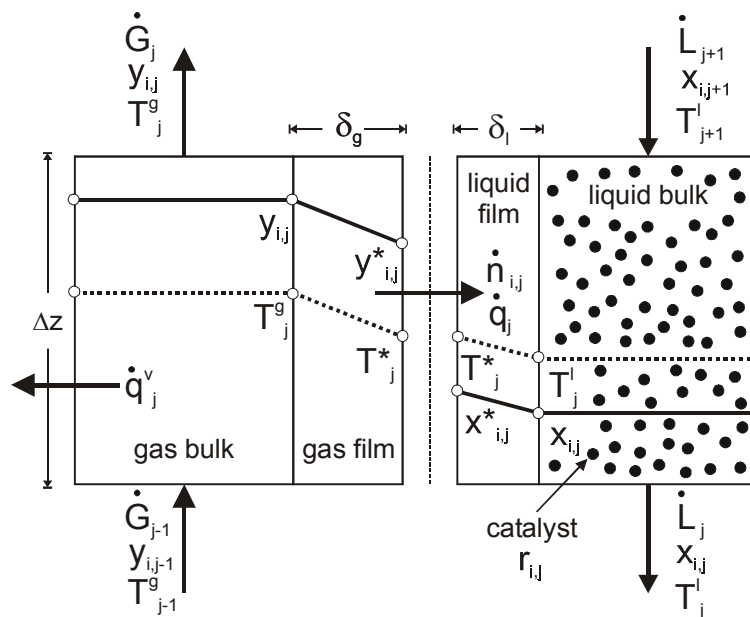


Figure 10: Two-film model for a reactive packing segment

Pöpken et al. [38] published an extensive experimental study on the reaction kinetics and chemical equilibrium of the system methanol / acetic acid // methyl acetate / water. They derived an adsorption-based model for the heterogeneously catalysed reaction choosing the ion exchange resin Amberlyst 15 (Rohm and Haas Co.) as catalyst. This model does not only consider thermodynamic non-idealities by using liquid phase activities for the reaction kinetic and equilibrium equations, but also sorption and swelling effects. The physical properties of Amberlyst 15 are very similar to those of Lewatit K2621 used here. However, the concentration of acid sites for dry Lewatit K2621 has been determined experimentally as  $4.55 \text{ mol}^{H^+}/g_{Cat}$ , close to the value of  $4.75 \text{ mol}^{H^+}/g_{Cat}$  reported for Amberlyst 15. Therefore, this model was adopted and for consistency, the UNIQUAC approach was used for vapour-liquid equilibrium with binary interaction parameters also taken from Pöpken et al. [38].

The component balances for the gas and liquid phase on a non-equilibrium stage  $j$  were written as

$$0 = \dot{G}_{j-1} \cdot y_{i,j-1} - \dot{G}_j \cdot y_{i,j} - \dot{n}_{i,j} \cdot a \cdot \frac{\pi}{4} \cdot d_C^2 \cdot \Delta z \quad i = 1 \dots n \quad (35)$$

$$0 = \dot{L}_{j+1} \cdot x_{i,j+1} - \dot{L}_j \cdot x_{i,j} + (\dot{n}_{i,j} \cdot a + r_{i,j} \cdot \psi \cdot \rho_{CB}) \cdot \frac{\pi}{4} \cdot d_C^2 \cdot \Delta z \quad i = 1 \dots n \quad (36)$$

The component balances are completed with the summation conditions for the mole fractions in both phases

$$\sum_{i=1}^n x_{i,j} = \sum_{i=1}^n y_{i,j} = 1 \quad (37)$$

The interfacial mass transfer rates have been calculated with the Maxwell-Stefan equations to account for diffusional interaction and thermodynamic non-idealities. To relate the multicomponent mass transfer rates to the binary mass transfer experiments described above, the method of Krishna and Standard [54] was used. The diffusional fluxes can be calculated from

$$(J) = -c_{t,G}^{av} \cdot [k_G^{av}] \cdot (y_{i,j}^* - y_{i,j}) = -c_{t,L}^{av} \cdot [k_L^{av}] \cdot [\Gamma_L^{av}] \cdot (x_{i,j} - x_{i,j}^*) \quad (38)$$

with the matrix of mass transfer coefficients defined as

$$[k^{av}] = [R^{av}]^{-1} \quad (39)$$

$$\text{with} \quad R_{ii} = \frac{y_i^{av}}{\kappa_{in}} + \sum_{\substack{k=1 \\ k \neq j}}^n \frac{y_k^{av}}{\kappa_{ik}} \quad \text{and} \quad R_{ij} = -y_i^{av} \cdot \left( \frac{1}{\kappa_{ij}} - \frac{1}{\kappa_{in}} \right) \quad i = 1 \dots n-1 \quad (40)$$

The binary mass transfer coefficients  $\kappa_{ij}$  can be derived from mass transfer correlations for binary systems, using the appropriate Maxwell-Stefan diffusion coefficient. For the reactive column section, the mass transfer correlation for MULTIPAK<sup>®</sup> were used. The mass transfer in the non-reactive sections was calculated according to Rocha et al. [49], using the geometrical characteristics of Montz-Pak A3-500.

The linearised theory of Toor, Stewart and Prober [55] can be applied to evaluate  $[R^{av}]$ ,  $[T^{av}]$  and all physical properties, using an average mole-fraction defined as

$$y_{i,j}^{av} = \frac{y_{i,j}^* + y_{i,j}}{2} \quad i = 1 \dots n \quad (41)$$

Phase equilibrium is assumed at the interface with interfacial compositions calculated from

$$y_{i,j}^* = K_{i,j}^{eq} \cdot x_{i,j}^* \quad i = 1 \dots n \quad (42)$$

with vapour-liquid equilibrium constants  $K_{i,j}^{eq}$  determined from the UNIQUAC equations and the extended Antoine equation for vapour pressure [56].

Since only  $n-1$  diffusional fluxes are independent, the energy balances for both phases including the conductive heat flux across the interface are formulated to relate the diffusional fluxes to the component molar fluxes [17]. They are written as follows:

$$0 = \dot{G}_{j-1} h_{G,j-1} - \dot{G}_j h_{G,j} - \left( \dot{q}_j^v + \dot{q}_j^* \frac{a d_C}{4} \right) \pi d_C \Delta z \quad i = 1 \dots n \quad (43)$$

$$0 = \dot{L}_{j+1} h_{L,j+1} - \dot{L}_j h_{L,j} + \dot{q}_j^* \frac{\pi}{4} a d_C^2 \Delta z \quad i = 1 \dots n \quad (44)$$

The heat transfer across the vapour-liquid interface consist of an convective and conductive part and can be calculated from

$$\dot{q}_j^* = -\frac{\lambda_G^{av}}{\delta_G} (T_j^* - T_{G,j}) + \sum_{i=1}^n \dot{n}_{i,j} h_{G,i,j} = -\frac{\lambda_L^{av}}{\delta_L} (T_{L,j} - T_j^*) + \sum_{i=1}^n \dot{n}_{i,j} h_{G,i,j} \quad (45)$$

The film thickness in both phases is needed to calculate the conductive interfacial heat transfer, but in multicomponent systems only individual film thicknesses  $\delta_{ij}$  can be derived from binary mass transfer coefficients.

$$\delta_{ij} = \frac{D_{ij}}{\kappa_{ij}} \quad (46)$$

Therefore, a mean film thickness has been defined as

$$\bar{\delta} = \frac{1}{n(n-1)} \sum_{i=1}^n \sum_{\substack{j=1 \\ j \neq i}}^n \delta_{ij} \quad (47)$$

This approximation is justified since all individual film-thickness are similar and the conductive heat transfer across the interface is negligible in comparison to the convective transfer. It has to be emphasised that the mean film thickness is only used to calculate the conductive heat transfer and not for the evaluation of individual mass transfer across the interface.

The segmentation of the catalytic distillation column in axial direction together with the detailed rate-based approach results in a complex and highly nonlinear algebraic system of equations. All model equations have been implemented in the commercial simulation environment Aspen Custom Modeler™. A first guess of the bulk phase

compositions and temperatures was provided by the solution of an equilibrium stage model without reactions. The first convergent initialisation of the rate-based approach was achieved by implementing effective diffusion coefficients, which leads to decoupled mass transfer equations. This simplified model has been extended by adding reaction terms and the Maxwell-Stefan approach.

## PILOT-PLANT EXPERIMENTS

Theoretical and experimental results for a the synthesis of methyl acetate via catalytic batch distillation with MULTIPAK<sup>®</sup> have already been presented by Kreul et al. [53]. To evaluate the influence of the packing characteristics on the process, a pilot-plant column as shown in Figure 11 has been build up to investigate the continuous process behaviour experimentally.

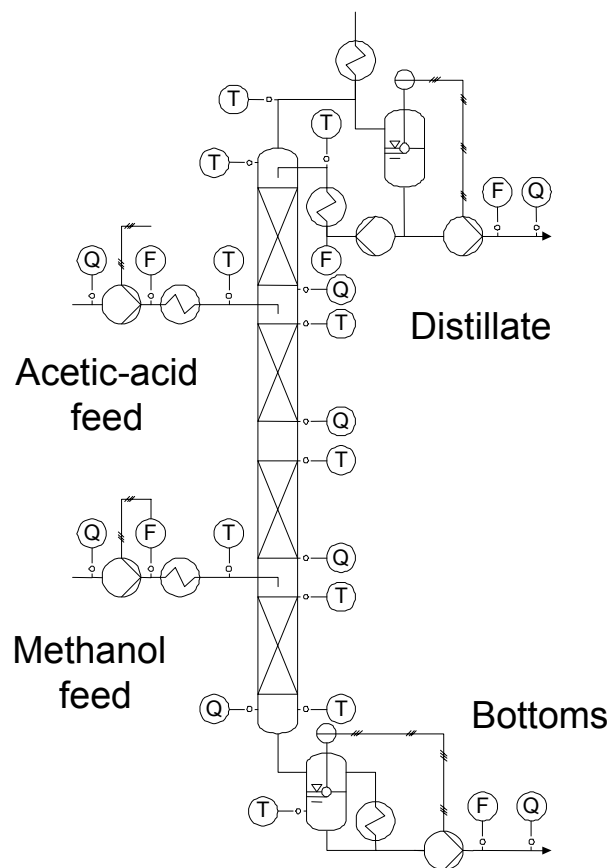


Figure 11: Catalytic distillation column.

The column design is similar to that presented by Krafczyk and Gmehling [51] or Bessling et al. [15] with an inner column diameter of 50 mm and an effective packing height of 4 m meter comprising 4 sections of 1 m each. A reactive section of 2 m is located in the middle of the column with two non-reactive sections of 1 m each below and above. The reactive section is equipped with MULTIPAK<sup>®</sup>-I and the non-reactive section with Montz-Pak A3-500. High conversion can only be achieved if the reactants can flow countercurrently in the reactive section [2], thus methanol is fed to

the column below the reactive section, while the acetic acid feed is located above the catalytic packing.

Special attention has been paid to allow for a comparison of experimental and theoretical process data. The flowrates of feed-, product- and reflux-streams are determined via mass flow measurements to ensure the accurate evaluation of process conditions. Liquid samples can be taken from all streams mentioned above as well as along the column height. The samples have been analysed by gaschromatography to determine the mass-fraction of all organic components and Karl-Fischer titration to ascertain the amount of water. Resistance thermometer have been installed for all in- and outlet streams and along the column height. This enables together with a heated jacket to prevent heat loss – a factor of great influence in small diameter columns – to draw an exact energy balance of the column. All data is recorded by a process control system and a data-reconciliation ensures the mass-balance of the column is fulfilled for all experimental runs.

A new series of experiments have been performed with a stoichiometric feed ratio of acetic acid and methanol. The reflux-ratio was kept constant at  $RR = 2.0$ , the feed-flowrate at  $3.0 \text{ kg/h}$  while the heat duty to the reboiler was varied over a wide range. A comparison of experimental results and model prediction is shown in Figure 11.

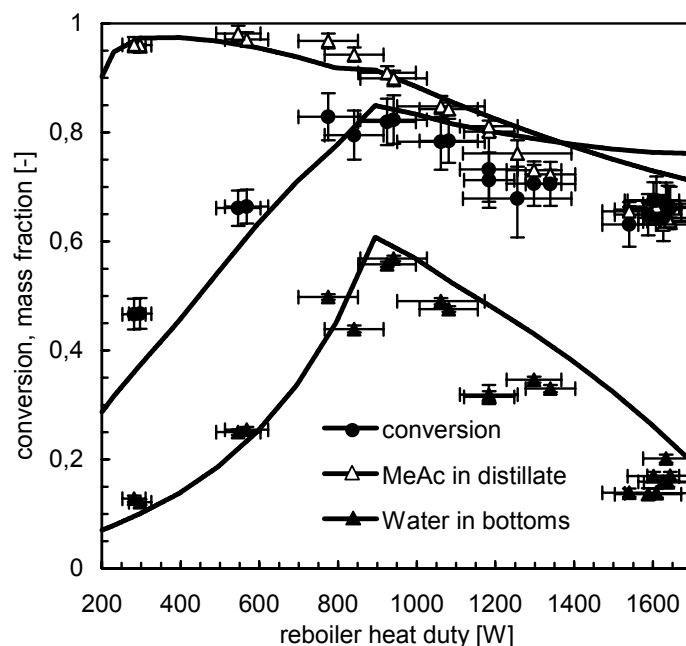


Figure 11: Model validation.

It can be seen that the process behaviour of the methyl acetate synthesis is well reflected by the simulation tool. Major deviations can only be observed at high reboiler duties, where water is enriched in the reactive part of the column and withdrawn with the distillate. Figure 13 shows the composition of the liquid phase along the column height, with process conditions according to a reboiler duty of  $880 \text{ W}$ . The theoretical values are displayed with continuous lines and empty symbols, while the experimental results for the samples taken along the column lines are shown by filled symbols.

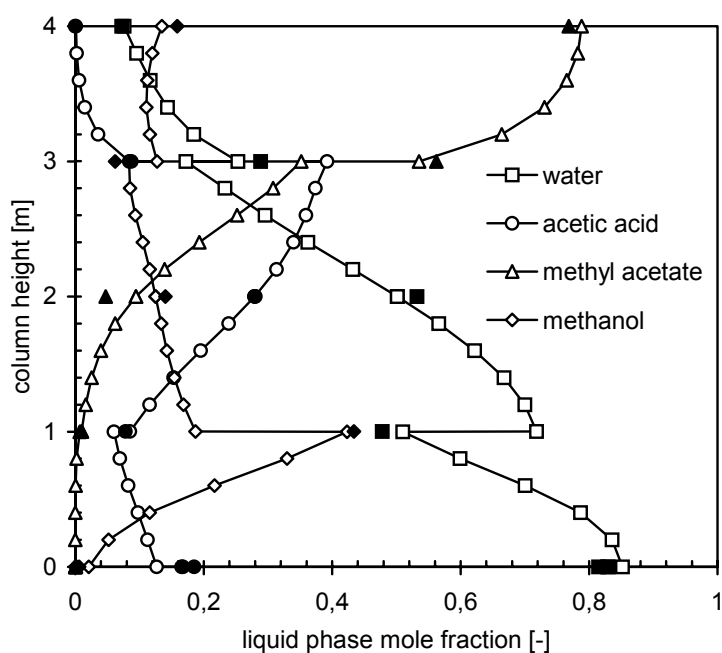


Figure 13: Liquid phase composition.

A maximum concentration of methanol and acetic-acid can be observed at the feed-locations respectively, while methyl acetate is enriched towards the top and water towards the bottom of the column. The experimental data verify that the simulation results reflect the real process behaviour for the methyl acetate synthesis with high accuracy.

## CONCLUSIONS

The main characteristics of the catalytic packing MULTIPAK<sup>®</sup> pressure drop, liquid holdup and separation efficiency have been determined experimentally for the whole loading range. A hydrodynamic model for this type of catalytic packing that takes the influence of the column diameter into account has been derived and compared with the experimental data. The good agreement confirms the assumptions which were made for the flow behaviour of gas and liquid. Additional experimental data for different types of MULTIPAK<sup>®</sup> are necessary to verify if the proposed model is valid for scale-up purposes.

A rigorous dynamic model based on the Maxwell-Stefan approach to describe mass transfer between phases has been modified and implemented in the simulation environment Aspen Custom Modeler<sup>™</sup>. By implementing the reaction kinetics and the hydrodynamics of the catalytic packings in the process simulation, their influence on design aspects of reactive distillation columns were taken into account. Steady-state simulations for the process of methyl acetate synthesis have been performed and compared with own experimental data from a pilot-scale reactive distillation column. It was shown that the process model is able to reflect the process behaviour for a variety of process conditions with minor deviations.

## ACKNOWLEDGEMENTS

The support from BASF AG, Bayer AG, Degussa AG, Siemens-Axiva GmbH and German Federal Ministry of Education and Research (Project No. 03C0306) is highly appreciated.

## NOMENCLATURE

$a$	specific packing surface	$\text{m}^2/\text{m}^3$
$c$	molar density	$\text{mol}/\text{m}^3$
$d$	diameter	$\text{m}$
$D$	diffusivity	$\text{m}^2/\text{s}$
$\mathcal{D}$	Maxwell-Stefan diffusivity	$\text{m}^2/\text{s}$
$F$	F-factor	$\text{kg}^{0.5}/\text{m}^{0.5}\text{s}$
$Fr$	Froude Number	
$f_s$	Wall factor	
$(J)$	vector of diffusion fluxes	$\text{mol}/\text{m}^2\text{s}$
$g$	gravitational acceleration	$\text{m}/\text{s}^2$
$\dot{G}$	gas mole flow	$\text{mol}/\text{s}$
$h$	specific enthalpy	$\text{J}/\text{mol}$
$h_L$	volumetric liquid holdup	
$H$	height	$\text{m}$
$HETP$	height equivalent of a theoretical plate	$\text{m}$
$HTU$	height of transfer unit	$\text{m}$
$k$	mass transfer coefficient	$\text{m}/\text{s}$
$K^{eq}$	vapour liquid equilibrium constant	
$\dot{L}$	liquid mole flow	$\text{mol}/\text{s}$
$m$	stripping factor	
$\dot{m}$	mass flow	$\text{kg}/\text{h}$
$n$	number of components	
$\dot{n}$	interfacial molar flux	$\text{mol}/\text{m}^2\text{s}$
$n_{th}$	number of theoretical stages	
$NTSM$	number of theoretical stages per meter	$1/\text{m}$
$\dot{q}$	heat flux	$\text{J}/\text{m}^2\text{s}$
$r$	reaction rate	$\text{mol}/\text{kg s}$
$[R]$	inverse mass transfer coefficient matrix	$\text{s}/\text{m}$
$Re$	Reynolds number	
$S$	corrugation side	$\text{m}$
$Sc$	Schmidt number	
$Sh$	Sherwood number	
$T$	temperature	$\text{K}$
$u$	velocity	$\text{m}/\text{s}$
$w$	mass fraction	
$x$	liquid phase mole fraction	
$y$	gas phase mole fraction	

## Greek Letters

$\alpha$	relative volatility	
$\beta$	mass transfer coefficient	m/s
$\delta$	film thickness	m
$\varepsilon$	void fraction	
$[\Gamma]$	matrix of thermodynamic correction factors	
$\eta$	viscosity	Pas
$\kappa$	individual mass transfer coefficients	m/s
$\lambda$	thermal conductivity	W/m K
$\theta$	inclination angle	
$\rho$	density	kg/m <sup>3</sup>
$\xi$	friction factor	
$\psi$	catalyst volume fraction	
$\Delta p$	pressure drop	Pa
$\Delta z$	segment height	m

## Subscripts

$B$	bottom
$C$	column
$CB$	catalyst bags
$D$	distillate
$eff$	effective
$eq$	equivalent
$F$	feed
$G$	gas phase
$i$	component index
$j$	segment index
$k$	component index
$L$	liquid phase
$LP$	Load point
$max$	maximum
$OG$	overall Gasphase
$OC$	open channel
$P$	Particle
$t$	total
$WG$	wire gauze sheets

## Superscripts

$av$	average
$v$	heat loss
*	at the interface

## REFERENCES

1. D.W. Agar (1999), Chem. Eng. Sci., 54, 1299-1305.
2. V. H. Agreda, L. R. Partin and W. H. Heise (1990), Chem. Eng. Prog., 86, 40-46.
3. J. L. DeGarmo, V. N. Parulekar and V. Pinjala (1992), Chem. Eng. Progr., 88, 43-50.
4. K. Rock, G. R. Gildert and T. McGuirk (1997), Chem. Eng., July, 78-84.
5. H. Spes (1966), Chemiker Ztg. / Chemische Apparatur, 90, 443-446.
6. I. Stankiewicz and J. A. Moulijn (2000), Chem. Eng. Prog., 96 (1), 22-34.
7. Beßling (1998), Zur Reaktivdestillation in der Prozeßsynthese, PhD Thesis, University of Dortmund, Germany.
8. J. R. Fair (1998), Chem. Eng., October, 158-162.
9. Górak and A. Hoffmann (2001), AIChE J., 47, 1067-1076.
10. R. Baur and R. Krishna (2002), Chem. Eng. Proc., 41, 445-462.
11. M. F. Doherty and G. Buzad (1992), Trans. IChemE, 70 448-458.
12. T. Frey and J. Stichlmair (1998). Chem.-Ing.-Tech., 70, 1373-1381.
13. M. J. Okasinski and M. F. Doherty (1997), AIChE J., 43, 2227-2238.
14. R. Taylor and R. Krishna (2000), Chem. Eng. Sci., 55, 5183-5229.
15. Bessling, J. M. Löning, A. Ohligschläger, G. Schembecker and K. Sundmacher (1998), Chem. Eng. Technol., 21, 393-400.
16. G. G. Podrebarac, F. T. T. Ng and G. L. Rempel (1998), Chem. Eng. Sci., 53, 1077-1088.
17. P. Higler, R. Taylor and R. Krishna (1999), Chem. Eng. Sci., 54, 1389-1395.
18. E. Kenig, K. Jakobsson, P. Banik, J. Aittamaa, A. Górak, M. Koskinen and P. Wettmann (1999), Chem. Eng. Sci., 54, 1347-1352.
19. K. Sundmacher and U. Hoffman (1996), Chem. Eng. Sci., 51, 2359-2368.
20. H. J. Bart and H. Landschützer (1996), Chem.-Ing.-Tech., 68, 944-946.
21. R. Schneider, C. Noeres, L. U. Kreul and A. Górak (2001), Comp. chem. Engng., 25, 169-176.

22. J. H. Lee, and M. P. Dudukovic (1998), *Comp. Chem. Engng.*, 23, 159-172.
23. G. G. Podrebarac, F. T. T. Ng and G. L. Rempel (1998), *Chem. Eng. Sci.*, 53, 1067-1075.
24. H. Subwalla, and J. R. Fair (1999), *Ind. Eng. Chem. Res.*, 38, 3696-3709.
25. Y. Zheng and X. Xu (1992), *Trans IChemE*, 70, 459-464.
26. X. Xu, Z. Zhao and S. Tian (1997), *Trans IChemE*, 75, 625-629.
27. H. Subwalla, J. C. Gonzalez, A. F. Seibert and J. R. Fair (1997), *Ind. Eng. Chem. Res.*, 36, 3821-3832.
28. Huang, G. G. Podrebarac, F. T. T. Ng and G. L. Rempel (1998), *Can. J. Chem. Eng.*, 76, 323-330.
29. P. Moritz, B. Bessling and G. Schembecker (1999), *Chem.-Ing.-Tech.*, 71, 131-135.
30. P. Moritz and H. Hasse (1999), *Chem. Eng. Sci.*, 54, 1367-1374.
31. J. Ellenberger and R. Krishna (1999), *Chem. Eng. Sci.*, 54, 1339-1345.
32. Górak, L. U. Kreul and M. Skowronski (1997), German patent 19701045 A1.
33. L. U. Kreul (1998), *Discontinuous and Reactive Distillation*, PhD. Thesis, University of Dortmund, Germany.
34. Noeres, A. Hoffmann and A. Gorak (2002), *Chem. Eng. Sci.*, *Article in press*.
35. Z. P. Xu and K. T. Chuang (1996), *Can. J. Chem. Eng.*, 74, 493-499.
36. Z. P. Xu, Z. P. and K. T. Chuang (1997), *Chem. Eng. Sci.*, 52, 3011-3017.
37. T. Pöpken, R. Geisler, L. Götze, A. Brehm, P. Moritz and J. Gmehling (1999), *Chem.-Ing.-Tech.*, 71, 96-100.
38. T. Pöpken, L. Götze and J. Gmehling (2000), *Ind. Eng. Chem. Res.*, 39, 2601-2611.
39. P. Moritz and H. Hasse (2001), *Chem.-Ing.-Tech.*, 73, 1554-1559
40. J. Mackowiak (1991), *Fluidodynamik von Kolonnen mit modernen Füllkörpern und Packungen für Gas/Flüssigkeitssysteme*, Salle/Sauerländer, Frankfurt a.M. pp. 148
41. J. G. Stichlmair, J. L. Bravo and J. R. Fair (1989), *Gas. Sep. & Pur.*, 3, 19-28
42. R. Billet (1995), *Packed Towers*, VCH, Weinheim, Germany, pp. 88-96

43. J. A. Rocha, J. L. Bravo and J. R. Fair (1993), *Ind. Eng. Chem. Res.*, 32, 641-651
44. U. Onken and W. Arlt (1990), *Recommended Test Mixtures for Distillation Columns*, The Institution of Chemical Engineers, Warwickshire, UK, pp. 31-36
45. J. G. Stichlmair and J. R. Fair (1998), *Distillation : principles and practice*, Wiley-VCH, New York, US, pp. 128
46. S. Pelkonen, R. Kaesemann and A. Górak (1997), *Ind. Eng. Chem. Res*, 36, 5392-5398
47. T. H. Chilton and A. P. Colburn (1935), *Ind. Eng. Chem.*, 27, 255-260
48. Ž. Olujić, A. B. Kamerbeek and J. de Graauw (1999), *Chem. Eng. Proc.*, 38, 683-695
49. J. A. Rocha, J. L. Bravo and J. R. Fair (1996), *Ind. Eng. Chem. Res.*, 35, 1660-1667
50. R. Taylor and R. Krishna (1993), John Wiley, New York, US
51. J. Krafczyk and J. Gmehling (1994), *Chem.-Ing. Tech.*, 66, 1372-1375
52. Z. P. Xu and K. T. Chuang (1996), *Can. J. Chem. Eng.*, 74, 493-500
53. L. U. Kreul, A. Górak, C. Dittrich and P. I. Barton (1998), *Comp. Chem. Engng.*, 22, Suppl., 371-378
54. R. Krishna and G. L. Standart (1979), *Chem. Eng. Commun.*, 3, 201-275
55. W. E. Stewart and R. Prober (1964), *Ind. Eng. Chem. Fundam.*, 4, 224-234
56. R. C. Reid, J. M. Prausnitz and B. E. Poling (1987), *The Properties of Gases & Liquids*, McGraw Hill, New York, US